Decoupling Crystallinity and Size of TiO2 Nanoparticles of TiO2: Application in Large Area Dye-Sensitized Solar Cells

Aiat Hegazy[1], Essam El-Shenawy[1] and Mohamed Abdelatef[1]

[1] National Research Centre, Cairo (Egypt)

Abstract

Dye-sensitized solar cells (DSSCs) have attracted great attention in recent years as a potential alternative to conventional silicon solar cells. However, a lot of current research is still focusing on enhancing their efficiency through the individual improvement of the DSSCs components, as well as their integration. Among these components, mesoporous TiO_2 plays an important role in the cell photoanode. Achieving well-crystallized small nanoparticles usually requires a room temperature synthesis, giving very small crystallites (4-10 nm) of TiO_2 anatase. As as-synthesized materials contain hydration water, a major drawback in DSSCs, we report how dehydration and crystallinity can be improved by annealing at a moderate temperature, without any sintering or significant particle coarsening. We report in this study a comprehensive study of the cell assembling, and its efficiency, characterized under AM 1.5 illumination with 100 mw/cm^2 light intensity.

Keywords: DSSC,TiO_2, nanoparticle, photovoltaic, anatase, solar cell, solar energy.

1. Introduction

Since their initial discovery (O'regan and Gratzel, 1991; Gratzel 2001) liquid-based dye-sensitized solar cells (DSSCs) are known as alternatives to conventional silicon-based photovoltaic devices. The first generation of liquid electrolyte-containing DSSCs display significant Power Conversion Efficiencies (PCE) > 14% (Mathew et al. 2014; Kakiage et al. 2015) at lab scale and 10% in module (Kazim et al. 2014), but the use of a liquid electrolyte becomes a burden for large-scale developments. Therefore, research on solid-state DSSCs (ss-DSSCs) has significantly increased over the last years reaching up 8.2% (Freitag et al. 2015) with the recent breakthrough of perovskites, especially organic-inorganic perovskites, which act as light harvester in place of organic dyes, and Hole Transporting Material (HTM)(Kazim et al. 2014). Nevertheless, TiO_2 anatase remains an important component in both types of DSSCs, as an electron collector. The reduction of interface transport resistance between all components is also a major requirement, which requires a high interfacial intimacy between components.

The electronic conduction in the protonated TiO_2 film, usually made of 20 nm TiO_2 particles, is the result of a complex mechanism in liquid DSSCs. First, the presence of both dye cations and iodine species, with the resulting formation of a positive layer on the surface of titania, create a Helmholtz double layer screening shell around the particles, which contributes to the reduction of the electron-hole recombination in TiO_2 (Cahen et al. 2000). It is also stated that the electrons are diffusing along the surface of the particles, as a result of a short screening Debye length (1.5 nm) (Cahen et al. 2000). If this limits the electron diffusion to a surface process for particles larger than 10 nm, we could wonder the effect of using smaller (sub-10 nm) nanoparticles, and if the whole volume will be used for conduction.

A major contributing factor to the efficiency of the titania-based photoanode is its structure, especially, the size of TiO_2 crystals. Although the reduction in crystal size influences positively the amount of dye adsorbed onto the surface and the dye-to-TiO_2 charge transfer, it affects negatively the total internal resistance of the cell as more grain boundaries are created per unit volume, reducing the light internal reflection. For example, it was demonstrated that mesoporous TiO_2 single crystals can deliver an enhanced mobility, good optoelectronic performances, and high material intimacy (Crossland et al. 2013).

doi:10.18086/swc.2017.20.05 Available at http://proceedings.ises.org

We prepared previously anatase nanocrystals at room temperature, as a result of synthesis parameters being finely optimized via a mixture design method (Hegazy and Prouzet, 2012). This nanopowder, already successfully tested for their photocatalytic properties, (Hegazy and Prouzet, 2013) could become the raw material for future roll-to-roll manufacturing of large-scale DSSCs, if the nanostructure can be dehydrated with thermal annealing without particle sintering or coarsening. As we demonstrated previously that the initial particle size can be preserved up to ≈ 400°C, (Hegazy and Prouzet, 2012) we decided to verify the efficiency of a dehydration treatment in this temperature range, and assess the photovoltaic properties of a DSSC assembled with this material. Different parameters in cell assembly were tested in order to improve the final structure and connectivity of the final TiO_2 photoanode. The influence of these parameters is reported in the present study, along with the assessment of our materials, in comparison with commercially available compounds assembled with the same method.

2. Experimental

2.1. Synthesis of TiO_2 nanoparticles

We reported the detailed study of this synthesis previously (Hegazy and Prouzet, 2012). This study allowed us to extrapolate the best composition, which would give both small nanocrystallites, and a pure anatase phase. This specific composition was chosen inside the composition mixture diagram giving the pure TiO_2 anatase phase. It corresponds to a composition between the (A) and (J) data points in the mixture phase diagram of our previous study (Hegazy and Prouzet, 2012).

2.2. Synthesis of the TiO_2 paste

The paste was prepared by mixing the TiO_2 nanopowder, with different organic additives used as plasticizers. Depending on their nature, we proceeded differently for their addition. In method 1, 0.35 g Pluronic™ P123, was dissolved into 5 mL EtOH, and then mixed with a suspension of 1.0 g of TiO_2 dispersed into 10 mL of EtOH. The resulting mixture was left at 100°C for 24 h, in a sealed vial. The vial was further cooled down before using the paste. In method 2, a mixture of Span™80/Tween™80 was prepared with the aim to obtain a final Hydrophilic Lipophilic Balance (HLB) of 13.6, (Hessien et al. 2012) and 0.035g of this mixture (equiv. one to two drops) was directly added into a suspension of 1g TiO2 in 10 mL acetic acid (N). The resulting paste was ground in a mortar to ensure good dispersion of the organics among the solid phase before being pasted.

2.3. Preparation of the TiO_2 film

The film was coated onto a FTO glass substrate, with doctor-blade method. The film thickness was controlled by the thickness of a 17 µm 3M adhesive tape, and the paste was spread with a glass rod over the space between the tape strips. The electrode was left to dry at 80°C for 3 hours. We cured organics used as plasticizers by either a thermal, or UV treatment. With the thermal treatment, the electrode was heated at 450°C for 30min, cooled down, and immersed into a 0.1M HCl aqueous solution for 2 hours. With UV treatment, the electrodes were exposed to an intense curing (300 W.inch^2) UV radiation for 20 min, before being immersed in the HCl solution. After analysis, we decided to combine both methods, and all electrodes used for the cell assembly, were made out of the TiO_2nanopowder, first annealed at 350°C for 4 hours, then cured at 450°C for 30 min, and exposed to UV. All electrodes were further grafted with the Z907 dye molecule. Adsorption of the dye was undertaken by immersing the TiO_2 electrode overnight in a 0.4 mM dye in 50:50 vol. t-butanol:acetronitrile solution. The grafted electrodes were finally washed with acetone to remove the excess of dye.

2.4. Counter electrode preparation

The presence of Pt nanoparticles at the surface of the counter-electrode is mandatory to achieve the reduction of the iodide/triiodide couple (Bonnemann et al. 2007). A commercial platinum paste (Platisol-T, Solaronix) was used as received and fired at 450°C for 30 min in order to remove organic binders. The electrode was immersed in DI water, before being sonicated for 20 minutes in ethanol, without any noticeable wrenching of the Pt layer from the substrate.

2.5. Cell assembly

The Pt electrode and the dye-adsorbed TiO_2 electrode were assembled as a sandwich-type, leading to a 5 cm^2 photoactive surface. The redox electrolyte was introduced to the cell by capillary action.

3. Results and discussions

3.1 Influence of treatment on structure of TiO_2

3.1.1 Thermal annealing

We have demonstrated in a previous study, that the crystallinity of as-synthesized TiO_2 anatase could be improved by a moderate thermal treatment without any dramatic change in the crystal size if the maximum temperature remained below 450°C (Hegazy and Prouzet, 2012). A fully dehydrated material is a compulsory requirement for use in DSSCs.

We analyzed by TEM the influence of annealing on the crystalline and particle structure for nanopowders annealed for 4 hours at 350 °C (Figure 1.a), 450°C (Figure 1.b), and 500°C (Figure 1.c). TEM diffraction reveals an improved crystallinity from 350 to 450°C (see figures inset), without drastic change in crystal size. HR-TEM investigation of the sample annealed at 450°C (Figure 1.d) confirms the formation of 10 nm average single crystal particles with high crystallinity. The inter-reticular distances of 3.62 Å and 2.1 Å correspond to the (101), and (200) planes, respectively. They are in the usual value range reported in literature for nanocrystalline TiO_2. The crystal size increases at 500°C (Figure 1.c), leading to well-defined diffraction patterns, which result from this size increasing.

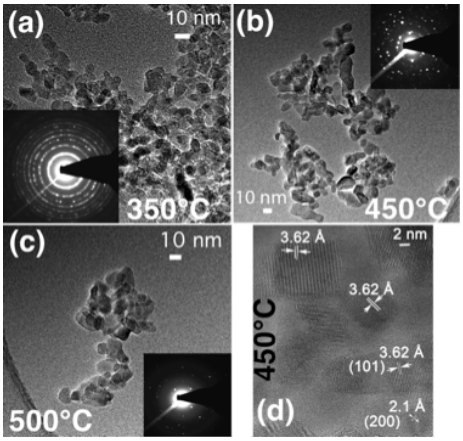

Figure 1: TEM micrographs and the corresponding diffraction patterns of nanocrystalline anatase TiO2 nanoparticles annealed at (a) 350 °C, (b) 450 °C, and (c) 500°C. (d) HR-TEM of TiO2

3.1.2 Organic additives

A TiO_2 paste was prepared with the addition of various organic additives used as binders: (i) Pluronic P123, (ii) PEG 12,000, or (iii) Span80/Tween20/acetic acid. These organics were chosen as plasticizers for facilitating the film formation. They were added to the anatase nanoparticles previously annealed at 350°C for 4 hours. As these organics must be removed after the film formation, we tested two types of curing, with a short thermal treatment (450°C, 30 min), or high intensity UV (300 W/in^2, 15 min). An observation by TEM (not shown) did not reveal any drastic change in the structure of titania particles, after either thermal or UV curing, irrespective of the type of additive.

Both surface area and porosity of the film are two important parameters in performance of DSSC, and porosity should be typically in the 50%-65% range (van de Lagemaat et al. 2001). Previous analyses showed that the small size of these nanoparticles create a significant textural porosity in the mesoporous range, with both specific surface area and porous volume changing with the thermal treatment (Hegazy and Prouzet 2012). We report in Figure 2, the N2 adsorption/desorption isotherms for the powder annealed at 350°C, and

the same powder prepared with the Span/Tween mixture plasticizing additive and cured either at 450°C, or under UV. Figure 3.a shows that all isotherms are rather similar (Type IV isotherms), with a steep adsorption between 0.6 and 0.9 of partial pressure. The specific surface area calculated via the multipoint BET model, gives values of 130, 160, and 200 $m^2.g^{-1}$ for the annealed, thermally cured, and UV cured samples, respectively. Their respective porous volume is 58% for the annealed powder, and 63% for both cured samples. The modeling of the pore size distribution (PSD), using the desorption isotherm, (Figure 2.b) allowed us to assess the possible influence of curing on the material porous structure. The initial PSD lies between 8 and 13 nm, and both materials after either thermal or UV curing, show only a slight broadening of PSD toward larger pores (8 – 18 nm range). We assign this PSD shift toward larger values, as a result of the organic additive that acts as a pore promoter and contributes to create some larger pores in addition to the initial PSD (the PSD is only broadened toward larger values, not fully shifted).

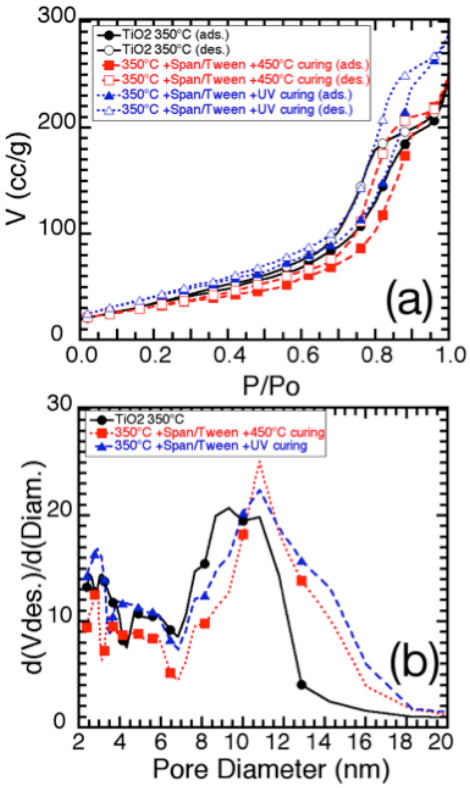

Figure 2: Nitrogen adsorption isotherms for the nanopowder after thermal annealing (350°C, 4h), and the same material after addition of the Span/Tween mixture additive, and either thermal (450°C, 30 min.) or UV (15 min) curing: (a) ads

3.2. Effect of dye absorption and photoelectronic properties onTiO_2 film

The cell performance is strongly affected by the efficiency of injected electrons from the dye to the conduction band of the TiO_2, which reflects the importance of the way the dye anchored to TiO_2 surface. As it has been demonstrated that both UV exposure and HCl treatment improve the photoanode properties, (Lee at al. 213; Hao et al. 2004). The thermally cured TiO_2 film was additionally activated under UV (10 min) and immersed into a 0.1 M hydrochloric aqueous solution for two hours, then rinsed with DI water until no acid trace could be found in washing water. The major effect of UV exposure is to reversibly create a high concentration of photoactive surface states, which were described as being continuously distributed below the conduction-band edge as shallow electron traps that would be beneficial for electron injection from the dye and transport by thermally activated detrapping (Lee at al.213; Hao et al. 2004; Tebby et al. 2009). The major effect of acid treatment is to increase the density of protonated sites, which favors multidentate dye adsorption. The actual influence of this HCl treatment is illustrated by comparing the UV-Vis spectra for both films prepared according to the procedure (thermally annealed and cured), and exposed to UV: adding an HCl treatment before dye adsorption, increases in the absorbance. A similar blue shift was observed for

all samples, which reveals a change in the electronic structure of the thin films surface, probably due to surface hydroxylation (Hao et al. 2004).

Figure 3 shows the J -V characteristics of the solar cell device made using thermally treated TiO_2/ plutonic P123 films at 450°C, the TiO_2 nanoparticles were preheated at 350°C. The photovoltaic parameters of the devices made using initially treated nanoparticles at 350°C and 450°C with and without HCl treatment. The short-circuit photocurrent density (Jsc) and the photoconversion efficiency (η) of the treated TiO_2 films are higher than those of the untreated counterparts, the active surface area was 5 cm^2 for all samples. After HCl treatment of the 350°C sample, the Jsc and η were increased by 28.4% and 4.5%, respectively. However, the open circuit voltage (Voc) was slightly changed and the fill factor (FF) was decreased. Whereas, for the sample prepared at 450°C, J_{sc} was increased by 36.3%, η by 37.2% and Voc by 8.6%. The poor FF is a result of a combination of the high series resistance (Rseries) and low shunt resistance (Rshunt). Figure 4 demonstrates that both devices made using our synthesized TiO_2 exhibit higher cell performance compared to the commercial ones. Although the sample prepared by surfactant and acetic acid displays higher efficiency than that made using pluronic, the later provides higher shunt resistance, Table 2.

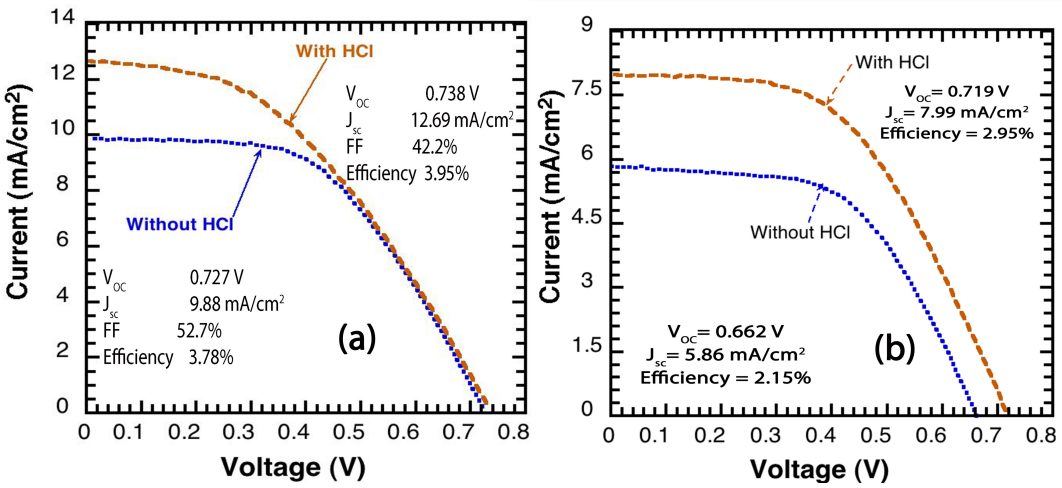

Figure 3: J-V curves for the comparison of the thermal and UV organic curing for nano powders being annealed beforehand at (a) 350°C, or (b) 450°C.

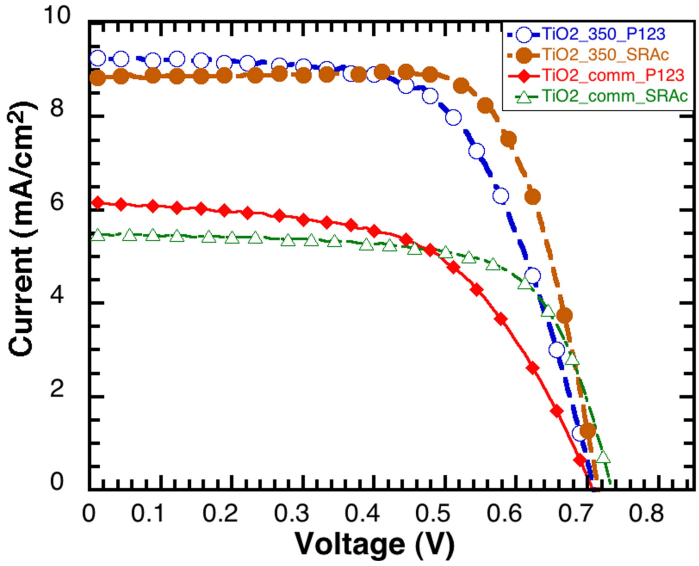

Figure 4: J-V curves of dye-sensitized TiO_2 films prepared on FTO/glass: with different organic additives to our nanopowder and the commercial one(active area=5 cm^2)

Table 1: Comparison between photovoltaic parameters of DSSCs prepared by the synthesized TiO_2 nanoparticles and the commercial TiO_2 counterparts.

Sample	V_{oc} (V)	J_{sc} (mA/cm^2)	*FF*	Efficiency %	R_s (Ω)	R_{sh} (Ω)
TiO_2_350°C_P123	0.713	9.43	62.6	4.21	16.6	1392
TiO_2_Degussa_P123	0.707	6.16	56.7	2.47	15.72	462
TiO_2_350°C_SRAc	0.72	8.41	77.1	4.67	2.21	324
TiO_2_Degussa_SRAc	0.734	5.47	68.9	2.77	4.12	606

Several DSSC devices were fabricated based on the TiO_2 films treated under different conditions. Unlike usual testing cells with an active surface area close to 1 cm^2, our cells were assembled with an active surface area of 5 cm^2, Fig.5 represents a picture of the tested cell. Therefore, the performances of the cells can hardly be compared to literature, and they were initially used as comparative within this study.

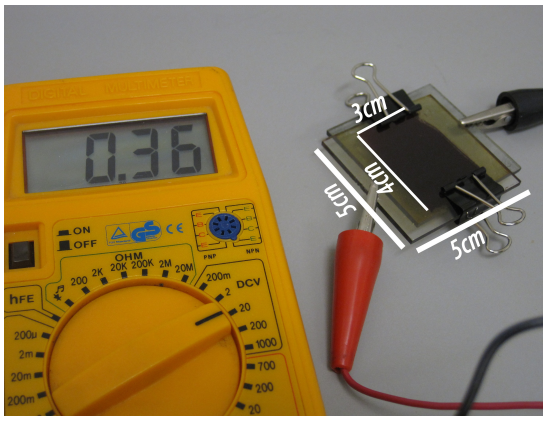

Figure 5 Picture of the full-assembled cell

The adsorption of Z907 Dye on the TiO_2 surface was characterized by ATR-FTIR spectroscopy. Figure 4 shows the ATR-FTIR absorption spectra of the Z907 dye adsorbed onto the TiO_2 surface. Many studies have shown that the dye anchors to the TiO_2 surface through different carboxylate anchoring modes, like physisorbed through hydrogen bonding, or chemisorbed via various types of chemical bonds (unidentate, bidentate, and bridging), with bridging and bidentate being the most stable ones (Lee et al. 2011; Leon et al. 2006; Wang et al. 2004).

Strong peaks were observed at 1,380 cm^{-1} and 1,613 cm^{-1} characteristics of the vsym (COO-) and vasym (COO-), respectively (Finnie et al.1998; Agrell et al. 2004). There is no indication of the presence of carboxylic bond at 1,716 cm-1. This indicates that the dye is anchored to the TiO_2 surface via bidentate or bridging not via unidentate mode. The saturated hydrocarbon chains are identified by the C-H stretch modes in the 2,800-3,000 cm^{-1} region with vibration modes of 2,852 cm^{-1} and 2,924 cm^{-1} for symmetric and asymmetric -CH_2-, respectively. The corresponding CH_3– peak is observed at 2,956 cm^{-1}. A broad absorption

peak is observed between 3,200-3,400 cm^{-1} (not displayed), corresponding to the –OH stretching modes of hydroxo and aquo ligands.

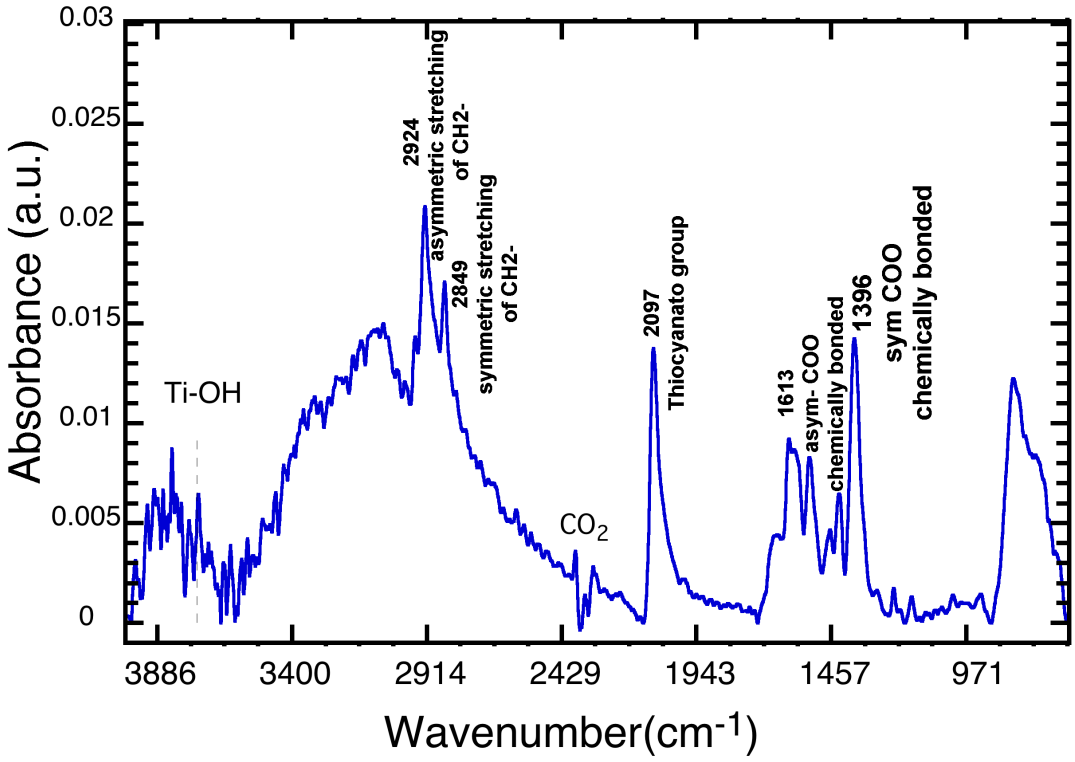

Figure5: FTIR spectrum of the TiO2- thin film after dye adsorption.

Another significant difference between our nanopowder and the commercial one is the strength of the dye adsorption. The samples prepared with Span/Tween show higher absorbance, which is consistent with the overall cell efficiency. All the reference cells made from the commercial TiO_2 exhibit lower absorbance, as a result of the dye being less adsorbed or easily removed before measurements. Our nanoparticles have the ability to keep 7 times more of dye after this process, than the commercial powder.

We performed an EIS analysis on different configurations to get more insights into the effect of resistances on the cell performance. We display the results obtained with TiO_2 films prepared with Span/Tween (Figure 5.a) or Pluronic P123 (Figure 5.b). A large semicircle can be observed in the Nyquist plot, which corresponds to the TiO2/dye/electrolyte triple interface. The interface between the high–frequency semicircle and the intermediate–frequency semicircle is difficult to distinguish due to the strong overlap of the charge transfer resistance on the TiO_2 surface and that on the Pt surface. A sub-circle in the low-frequency response is observed, which accounts for the contribution of the diffusion of the electro-active species in the liquid electrolyte (Longo et al. 2004). In the dark, the solar cells showed high impedance and the time constants are not well defined. For all devices testes (see Table 2), almost all the impedance parameters show a difference between illuminated and non-illuminated cells. The response at the intermediate interface under dark condition is much higher than the one under illumination, which corresponds to a high capacitance because of the expected accumulation of electrons and redox species at this interface (Nogeira et al.2004). From our results, it appears that the cells prepared with span/Tween exhibit a longer electron lifetime than those prepared with Pluronic(P123). The reference cells (commercial TiO_2 powder) showed an electron lifetime half times shorter electrons for recombination under illumination compared to the cells made with our

nanocrystalline TiO_2 material. Higher electron lifetime leads to significant electron transfer, and thus, an improved Jsc. Therefore, EIS analysis confirms the promising results obtained with cells assembled with our synthesized nanocrystalline material.

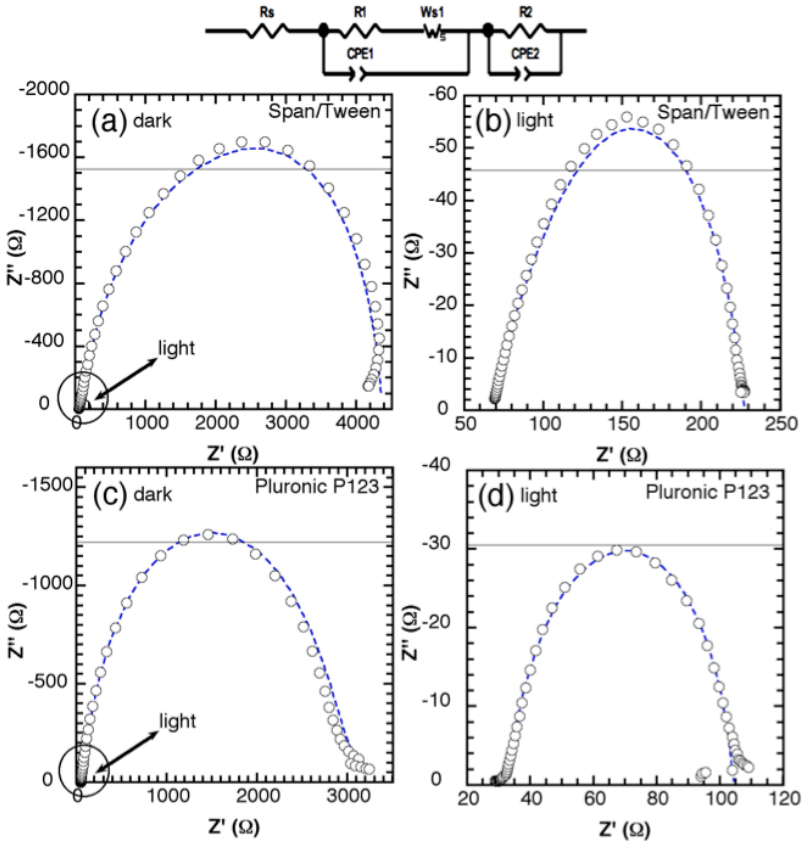

Figure 5: Nyquist representation of the impedance data obtained for Z907 dye–sensitized TiO2 solar cells prepared with preheated nanoparticles at 350oC mixed with (a,b) Span/Tween, (c,d) Pluronic P123, measured in the dark (a,c) or under light (b,d). The symbols represent the experimental data and the dashed lines correspond to the fitting obtained with View software using the displayed equivalent circuit displayed.

Sample	Area (cm^2)	R_s, Ωcm^{-2}	$R_{1(CE)}$, Ωcm^{-2}	T_1*10^6	P_1	$R_{2(REC)}$, Ωcm^{-2}	T_2*10^5	P_2	*Ws*, Ωcm^{-2}	τ_r/ms
AP_light	1	23.53	2.266	9.831	0.862	39.97	0.269	0.985	*39.35*	63
AP_light	1.5	48.45	1.908	0.405	1.023	23.48	1.893	1.043	47.27	35
AS_light	2.5	67.95	$1.7*10^{-7}$	0.195	0.6117	79.21	6.14	.9174	81.2	189

RP_light	1.2	37.4	0.586	3.041	0.966	59.31	1.034	.985	27.37	35

Table 2: Electrochemical parameters of DSSC prepared with different TiO2 films and organic additives. 'A' refers to the synthesized TiO2 nanoparticles prepared with S (Span/Tween) or P (Pluronic) additives, 'R' refers to reference electrodes prepared with TiO2 Degussa with S or P additives

4. Summary

In summary, we have successfully synthesized small crystalline TiO_2 nanoparticles by a novel soft chemistry method and investigated their properties in dye–sensitized solar cells. We also demonstrated that different organic additives can be used to prepare the photoanode and obtain the well defined working range of the porosity. The effect of UV exposure on the structure and crystal size of as-synthesized TiO_2 nanoparticles was tested through the XRD and N_2 isotherm characterization, which indicates no change in the crystal size and a higher surface area, respectively. Furthermore, various treatment methods (UV alone, thermal treatment alone, and combination of both) were applied. Although, UV treatment is able to clean the TiO_2 surface from organic contaminates, it is less efficient to be used alone, and leads to lower performance of solar cells, compared to thermal treatment. Interestingly, when it is used after the thermal treatment, the cells seem to show better efficiency, which will have to be confirmed in the future with more tests. The HCl treatment increases the cell efficiency by almost one to three. The enhancement was attributed to the increase of the amount of the dye. An intensive investigation on the effect of HCl on the adsorbed dye was done by the FTIR analysis. More investigation on the dye by the FTIR, demonstrates that the dye anchored chemically to TiO_2 surface. The amount of adsorbed dye for our TiO_2 films was 6 times compared to the amount of the commercial ones. The internal resistance of the cells were checked with EIS analysis, which shows higher electron lifetime, smaller charge transfer resistance for counter electrode and high recombination resistance compared to the commercial cells.

5. References

[1] Agrell, H. G., J. Lindgren, A. Hagfeldt, 2004. Coordinative interactions in a dye-sensitized solar cell, Journal of Photochemistry and Photobiology A: Chemistry, 164, 23-27.

[2] Bonnemann, H., G. Khelashvili, S. Behrens, A. Hinsch, K. R. Skupien, E. Dinjus, 2007. Role of the platinum nanoclusters in the iodide/triiodide redox system of dye solar cells, Journal of Cluster Science, 18, 141-155.

[3] Broekhoff, J. C. P., J. H. De Boer, 1968. Studies on pore systems in catalysts. Xiii. Pore distributions from the desorption branch of a nitrogen sorption isotherm in the case of cylindrical pores. B. Applications, Journal of Catalysis, 10, 377-390.

[4] Broekhoff, J. C. P., J. H. De Boer, 1968. Studies on pore systems in catalysts. Xii. Pore distributions from the desorption branch of a nitrogen sorption isotherm in the case of cylindrical pores. A. An analysis of the capillary evaporation process, Journal of Catalysis, 10, 368-374.

[5] Cahen, D., G. Hodes, M. Gratzel, J.-F. Guillemoles, I. Riess, 2000. Nature of photovoltaic action in dye-sensitized solar cells, J. Phys. Chem. B, 104, 2053-2059.

[6] Crossland, E. J. W., N. Noel, V. Sivaram, T. Leijtens, J. A. Alexander-Webber, H. J. Snaith, 2013. Mesoporous tio2 single crystals delivering enhanced mobility and optoelectronic device performance, Nature, 495, 215-219.

[7] Fang, X., T. Ma, G. Guan, M. Akiyama, E. Abe, 2004. Performances characteristics of dye-sensitized solar cells based on counter electrodes with pt films of different thickness, Journal of Photochemistry and

Photobiology a-Chemistry, 164, 179-182.

[8] Finnie, K. S., J. R. Bartlett, J. L. Woolfrey, 1998. Vibrational spectroscopic study of the coordination of (2,2 '-bipyridyl-4,4 '-dicarboxylic acid)ruthenium(ii) complexes to the surface of nanocrystalline titania, Langmuir, 14, 2744-2749.

[9] Freitag, M., Q. Daniel, M. Pazoki, K. Sveinbjörnsson, J. Zhang, L. Sun, A. Hagfeldt, G. Boschloo, 2015. High-efficiency dye-sensitized solar cells with molecular copper phenanthroline as solid hole conductor, Energy & Environmental Science, 8, 2634-2637.

[10] Gratzel, M., 2001. Photoelectrochemical cells, Nature, 414, 338-344.

[11] Hao, S., J. Wu, L. Fan, Y. Huang, J. Lin, Y. Wei, 2004. The influence of acid treatment of tio 2 porous film electrode on photoelectric performance of dye-sensitized solar cell, Solar Energy, 76, 745-750.

[12] Hegazy, A., E. Prouzet, 2012. Room temperature synthesis and thermal evolution of porous nanocrystalline TiO_2 anatase, Chemistry of Materials, 24, 245-254.

[13] Hegazy, A., E. Prouzet, 2013. Effect of physical chemistry parameters in photocatalytic properties of TiO_2 nanocrystals, Comptes Rendus Chimie, 16, 651-659.

[14] Hessien, M., N. Singh, C. Kim, E. Prouzet, 2011. Stability and tunability of o/w nanoemulsions prepared by phase inversion composition, Langmuir, 27, 2299-2307.

[15] Hirose, F., K. Kuribayashi, M. Shikaku, Y. Narita, Y. Takahashi, Y. Kimura, M. Niwano, 2009. Adsorption density control of n719 on TiO_2 electrodes for highly efficient dye-sensitized solar cells, J. Electrochem. Soc., 156, B987-B990.

[16] Jaroniec, M., 1995. Evaluation of the fractal dimension from a single adsorption isotherm, Langmuir, 11, 2316-2317.

[17] Kakiage, K., Y. Aoyama, T. Yano, K. Oya, J.-I. Fujisawa, M. Hanaya, 2015. Highly-efficient dye-sensitized solar cells with collaborative sensitization by silyl-anchor and carboxy-anchor dyes, Chemical Communications, 51, 15894-15897.

[18] Kang, S. H., J.-Y. Kim, H. S. Kim, H.-D. Koh, J.-S. Lee, Y.-E. Sung, 2008. Influence of light scattering particles in the TiO_2 photoelectrode for solid-state dye-sensitized solar cell, Journal of Photochemistry and Photobiology A: Chemistry, 200, 294-300.

[19] Kazim, S., M. K. Nazeeruddin, M. Gratzel, S. Ahmad, 2014. Perovskite as light harvester: A game changer in photovoltaics, Angew. Chem.-Int. Edit., 53, 2812-2824.

[20] Kopidakis, N., K. D. Benkstein, J. Van De Lagemaat, A. J. Frank, 2003. Transport-limited recombination of photocarriers in dye-sensitized nanocrystalline tio2 solar cells, J. Phys. Chem. B, 107, 11307-11315.

[21] Lee, M.-K., H. Yen, C.-C. Hsiao, 2011. Efficiency improvement of dye-sensitized solar cell with ultraviolet and hydrogen chloride treatments, J. Electrochem. Soc., 158, K136-K139.

[22] Leon, C. P., L. Kador, B. Peng, M. Thelakkat, 2006. Characterization of the adsorption of ru-bpy dyes on mesoporous TiO_2 films with uv-vis, raman, and ftir spectroscopies, Journal of Physical Chemistry B, 110, 8723-8730.

[23] Longo, C., M.-A. De Paoli, 2003. Dye-sensitized solar cells: A successful combination of materials, J. Braz. Chem. Soc., 14, 889-901.

[24] Mathew, S., A. Yella, P. Gao, R. Humphry-Baker, B. F. Curchod, N. Ashari-Astani, I. Tavernelli, U. Rothlisberger, M. K. Nazeeruddin, M. Grätzel, 2014. Dye-sensitized solar cells with 13% efficiency achieved through the molecular engineering of porphyrin sensitizers, Nature Chemistry, 6, 242-247.

[25] Hara, K. and Arakawa, H. (2003) Dye-Sensitized Solar Cells, in Handbook of Photovoltaic Science and Engineering (eds A. Luque and S. Hegedus), John Wiley & Sons, Ltd, Chichester, UK. doi: 10.1002/0470014008.ch15

[26] Nogueira, A. F., C. Longo, M. A. De Paoli, 2004. Polymers in dye sensitized solar cells: Overview and perspectives, Coordination Chemistry Reviews, 248, 1455-1468.

[27] O'regan, B., M. Gratzel, 1991. A low-cost, high-efficency solar-cell based on dye-sensitized colloidal tio2 films, Nature, 353, 737-740.

[28] Prouzet, E., C. Boissière, S. S. Kim, T. J. Pinnavaia, 2009. Roughness of mesoporous silica surfaces deduced from adsorption measurements, Microporous Mesoporous Mat., 119, 9-17.

[29] Prouzet, E., F. Cot, G. Nabias, A. Larbot, P. J. Kooyman, T. J. Pinnavaia, 1999. Assembly of mesoporous silica molecular sieves based on nonionic ethoxylated sorbitan esters as structure directors, Chemistry of Materials, 11, 1498-1503.

[30] Shao, W., F. Gu, C. Li, M. Lu, 2010. Interfacial confined formation of mesoporous spherical tio2 nanostructures with improved photoelectric conversion efficiency, Inorg. Chem., 49, 5453-5459.

[31] Tebby, Z., O. Babot, D. Michau, L. Hirsch, L. Carlos, T. Toupance, 2009. A simple route towards low-temperature processing of nanoporous thin films using uv-irradiation: Application for dye solar cells, Journal of Photochemistry and Photobiology a-Chemistry, 205, 70-76.

[32] Van De Lagemaat, J., K. D. Benkstein, A. J. Frank, 2001. Relation between particle coordination number and porosity in nanoparticle films: Implications to dye-sensitized solar cells, J. Phys. Chem. B, 105, 12433-12436.

[33] Wang, P., S. M. Zakeeruddin, J. E. Moser, R. Humphry-Baker, P. Comte, V. Aranyos, A. Hagfeldt, M. K. Nazeeruddin, M. Gratzel, 2004. Stable new sensitizer with improved light harvesting for nanocrystalline dye-sensitized solar cells, Advanced Materials, 16, 1806.